THE JOURNAL OF PHYSICAL CHEMISTRY A

Article

pubs.acs.org/JPCA

Electronic Structure and Optical Properties of the Thiolate-Protected $Au_{28}(SMe)_{20}$ Cluster

Stefan Knoppe,*[,†] Sami Malola,[‡] Lauri Lehtovaara,[§] Thomas Bürgi,[∥] and Hannu Häkkinen[‡,§]

[†]Molecular Imaging and Photonics, Department of Chemistry, KU Leuven, Celestijnenlaan 200D, 3001 Heverlee, Belgium
[‡]Department of Physics and [§]Department of Chemistry, Nanoscience Center, University of Jyväskylä, FI-40014 Jyväskylä, Finland
[∥]Department of Physical Chemistry, University of Geneva, 30 Quai Ernest-Ansermet, 1211 Geneva 4, Switzerland

Supporting Information

ABSTRACT: The recently reported crystal structure of the $Au_{28}(TBBT)_{20}$ cluster (TBBT: *p-tert*-butylbenzenethiolate) is analyzed with (time-dependent) density functional theory (TD-DFT). Bader charge analysis reveals a novel trimeric $Au_3(SR)_4$ binding motif. The cluster can be formulated as $Au_{14}(Au_2(SR)_3)_4(Au_3(SR)_4)_2$. The electronic structure of the Au_{14}^{6+} core and the ligand-protected cluster were analyzed, and their stability can be explained by formation of distorted eight-electron superatoms. Optical absorption and circular dichroism (CD) spectra were calculated and compared to the experiment. Assignment of handedness of the intrinsically chiral cluster is possible.

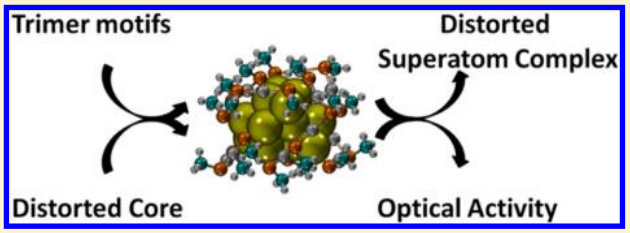

INTRODUCTION

The structure determination of thiolate-protected gold clusters $[Au_m(SR)_n]^z$ (SR, thiolate; *z*, charge) of atomic precision (less than ca. 200 Au atoms) is of high importance for understanding their stability and forms the basis for applications in, for instance, catalysis, sensing, and drug delivery.[1−5] Moreover, a deeper insight into their electronic structures aids in determining the transition from molecular to collective behavior (emergence of localized surface plasmon resonances). In recent years, a number of gold clusters has been characterized by means of X-ray structure determination, e.g., Au_{102}(*p*-MBA)$_{44}$ (*p*-MBA: *p*-mercaptobenzoic acid),[6] $[Au_{25}$(2-PET)$_{18}]^{0/1-}$ (2-PET: 2-phenylethylthiolate),[7,8] Au_{38}(2-PET)$_{24}$,[9] and $Au_{36}(TBBT)_{24}$.[10] Very recently, the structure of $Au_{28}(TBBT)_{20}$ was solved by Jin and co-workers.[11]

A common feature of these clusters is the fact that the thiolate ligands do not bind in a terminal fashion to the core of the clusters. Instead, two thiolate ligands stabilize a Au adatom, forming oligomeric units $Au_x(SR)_{x+1}$ (x = 1, 2). This "divide-and-protect" feature has been predicted from computational studies.[12] As yet, only monomeric (x = 1) and dimeric (x = 2) units were characterized without doubt. Computational studies, however, predict also trimeric (x = 3) units for very small clusters (less than 20 Au atoms).[13−15] A facile explanation for the stability of thiolate-protected clusters is given by the Superatom Complex Model (SACM),[16] an extension of the well-known superatom model that explains the stability of certain magic number-sized bare metal clusters in the gas phase.[17−20] In principle, a cluster is expected to exhibit electronic stabilization when the number of valence electrons in the cluster, $N_e = m - n - z$, is a magic number (2, 8, 18, 34, 58, ...). It should be noted that this model is based on cluster cores with spherical geometry, e.g., icosahedra. The rule is fulfilled for $[Au_{25}(SR)_{18}]^-$ (N_e = 8) and $Au_{102}(SR)_{44}$ clusters (N_e = 58). The $Au_{38}(SR)_{24}$ cluster (N_e = 14) was found to have a prolate Au_{23} core, and its stability can be explained as a "supermolecule" because two 7-electron units form superatom-bonding (Super-F_2) or alternatively can be explained by considering a subshell closing at 14 valence electrons in a strongly prolate-deformed metal core.[21−24] The stability of $Au_{40}(SR)_{24}$ (N_e = 16) can be explained by a dimer of 8-electron superatoms.[25]

A series of thiolate-protected gold clusters ($Au_{102}(SR)_{44}$, $Au_{38}(SR)_{24}$, and $Au_{28}(SR)_{20}$) was found to bear intrinsic chirality due to the arrangement of the (achiral) thiolate ligands (protecting units $Au_x(SR)_{x+1}$) on the surface of the cluster core.[6,9,11,22] Recently, it was demonstrated that it is possible to separate the enantiomers of Au_{38}(2-PET)$_{24}$ clusters and their circular dichroism (CD) spectra were measured.[26] Similarly, the Au_{40}(2-PET)$_{24}$ cluster was separated into enantiomers.[27] The CD spectra provide a deeper insight into the electronic structure of the clusters, because they typically resolve more electronic transitions than ordinary absorption spectra. It should be noted that the clusters were stabilized with achiral ligands and that the chirality, hence optical activity, solely arises from the arrangement of the ligands on the cluster surface. The optical activity is, therefore, strictly associated with the structure of the cluster itself, in contrast to the use of chiral ligands, which induce optical activity to virtually any cluster size.[28−34] The optical activity of Au_{40}(2-PET)$_{24}$ allowed for a detailed prediction of the structure of the cluster.[25]

Received: July 27, 2013
Revised: September 12, 2013
Published: September 13, 2013

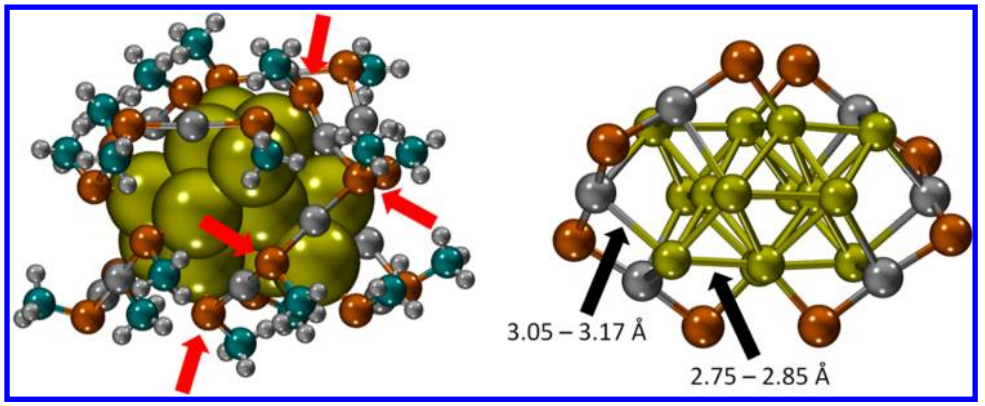

Figure 1. Left: structure of the optimized $Au_{28}(SMe)_{20}$ cluster. Red arrows point at sulfur atoms assigned to one of the trimeric units (see text). Right: comparison of Au−Au distances of atoms within the core (yellow, 2.75−2.85 Å) and between core atoms and those assigned to trimeric units (gray, 3.05−3.17 Å). The slightly larger distances for the latter point toward a "divide-and-protect" interpretation. Colors: yellow, Au (core); gray, Au (adatom); orange, sulfur; blue, carbon; white, hydrogen.

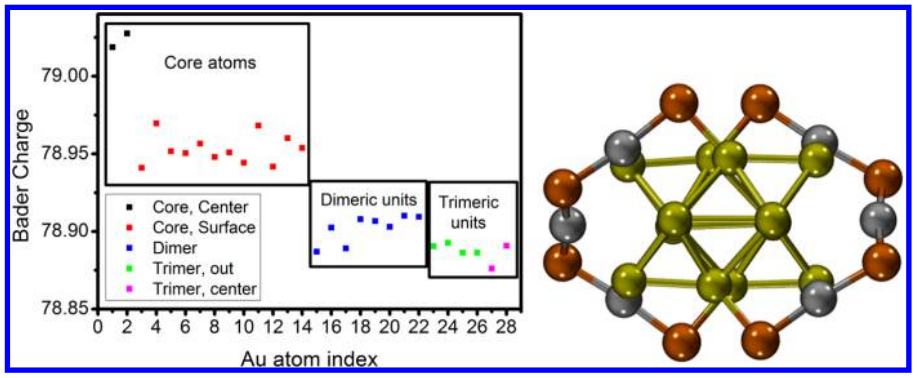

Figure 2. Left: Bader charges of the Au atoms in the $Au_{28}(SMe)_{20}$ cluster (PBE functional). A very similar trend is observed for the structure optimized with the LDA functional (Figure S-1, Supporting Information). The first 14 atoms (ascribed to the core) have distinctively higher Bader charges than the remaining 14 atoms (which are associated with the protecting units). Right: trimer motifs identified according to their Bader charges. Colors: yellow, Au (core); gray, Au (adatom); orange, sulfur.

We herein report a computational study of the recently solved structure of the $Au_{28}(TBBT)_{20}$ cluster.[11] We optimized the structure of a model cluster, $Au_{28}(SMe)_{20}$, and calculated both absorption and circular dichroism spectra of the right-handed enantiomer with state-of-the-art TD-DFT. This allows assignment of handedness by comparison with experimental CD spectra. Bader charge analysis predicts the existence of trimeric protecting units, hence giving rise to a Au_{14} kernel of the cluster. The electronic structures of the Au_{14} core and the ligand-protected cluster were analyzed in the context of the superatom complex model (SACM).

■ COMPUTATIONAL METHODS

For modeling we used density-functional theory with projector augmented waves (PAW) as implemented in the real-space grid code-package GPAW.[35,36] Scalar-relativistic effects for Au are considered in the PAW setup. Optimization of the $Au_{28}(SR)_{20}$ cluster (R: CH_3) was performed with a grid spacing of 0.2 Å until the remaining forces on each atom were below 0.05 eV/Å. All calculations were performed at the GGA-PBE level.[37,38] For comparison, the structure was optimized with the LDA functional, too. Bader charges were calculated using the program provided by the Henkelman group.[39,40] For TD-DFT, the electronic structure of the cluster was calculated including a sufficient range of unoccupied electronic states. Oscillator and rotatory strengths were calculated with an updated code of the recent implementation of circular dichroism spectra into GPAW.[25] Spectra were folded with a Gaussian broadening of 0.1 eV. Angular momentum resolved projected density of states analysis was performed by projection to the center of mass of the structures.[16] Kohn−Sham (KS) wave functions were visualized with an isosurface cutoff of 0.05.

■ RESULTS AND DISCUSSION

We optimized the structure of the $Au_{28}(SR)_{20}$ cluster using R = −Me to minimize the cost of the computations. The PBE-optimized structure is shown in Figure 1. Jin and co-workers note a novel binding motif in the structure of the cluster.[11] According to this, the cluster consists of a Au_{20} kernel that is protected by four dimeric $Au_2(SR)_3$ units. The remaining eight thiolate groups are characterized as binding directly to the surface of the Au_{20} kernel. This situation is very similar to the one interpreted for $Au_{36}(SR)_{24}$.[10] A closer look to the structure and the gold atoms on the surface that neighbor the respective sulfur atoms shows that these are slightly detached from the surface of the core. We analyzed the Bader charges (BC) of all atoms in the cluster. If the gold atoms on the surface next to the "isolated" thiolate groups would belong to the core, a charge close to 0 would be expected. According to the divide-and-protect concept,[12] the adatoms stabilized between two thiolate groups are expected to be oxidized (formal charge +1).

dx.doi.org/10.1021/jp407494v | J. Phys. Chem. A 2013, 117, 10526−10533

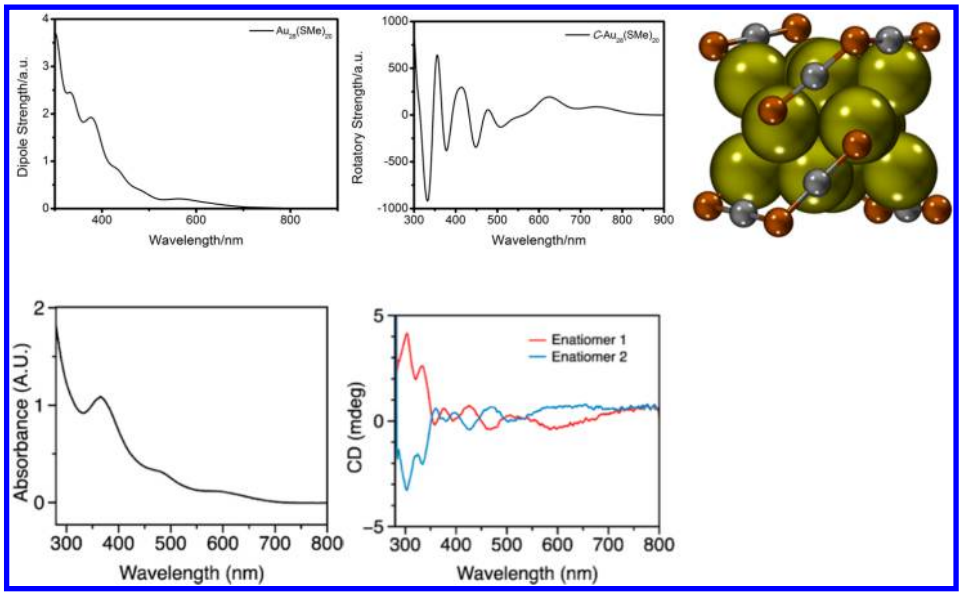

Figure 3. Top: simulated absorption (left) and circular dichroism (center) spectra of the $Au_{28}(SMe)_{20}$ cluster. A Gaussian line broadening of 0.1 eV was applied. Top, right: handedness of the calculated enantiomer of the $Au_{28}(SR)_{20}$ cluster. The right-handed *C*-enantiomer is shown, which was also used for computing the CD spectrum. The trimeric units and organic rests are removed for clarity. Colors: yellow, Au (core); gray, Au (adatom); orange: sulfur. Bottom: experimental absorption and CD spectra as reported in ref 11. Adapted with permission from ref 11. Copyright (2013) American Chemical Society.

BC analysis of the Au atoms reveals a distribution of charges. Fourteen Au atoms possess a slightly higher charge (average BC 78.963 |e| corresponding to +0.037 |e| per atom) than the other fourteen atoms (average BC 78.896 corresponding to +0.104). Lower Bader charges (i.e., higher net positive charges) indicate oxidation of the respective atoms. Although the prior ones are easily identified as those belonging to the core (the two atoms with highest BC are found in the center of the core), eight of the latter ones are the adatoms belonging to the four dimeric units. The remaining six Au atoms have charges very similar to those found for the adatoms in the dimeric units. On this basis, we assign these six atoms to trimeric protecting units $Au_3(SR)_4$. An overview of the Bader charges found for the Au atoms is found in Figure 2. Bader charges of the structure optimized with the LDA functional show the same trend (Figure S-1, Supporting Information). The PBE-functional tends to overestimate bond lengths and may therefore exaggerate the Bader charges. The LDA-functional gives bond distances closer to the experimental structure. A similar trend in the Bader charges of the Au atoms gives additional confidence in our assignment. In addition, the Au−Au distances of the atoms in question also point toward their interpretation as adatoms: whereas the distances between the atoms in the core are in the range of ca. 2.75−2.85 Å, the adatoms in the trimer motifs are slightly more detached from the core atoms (selected structural parameters of both the experimental and optimized structures are listed in the Supporting Information, Table S-1). Their nearest neighbors (Au atoms) fall within 3.05−3.17 Å. The trimeric units (Figure 2, right) are distorted as compared to dimeric or monomeric units. The Au(I)−S−Au(I) angles fall within 90−95°, the Au(0)−S−Au(I) angles are about 95°. This leads to a zigzag arrangement of the oligomeric structure. Very similar to dimeric and monomeric units, the trimer motifs show linear S−Au(I)−S angles (close to 180°). The distortion seems to arise from the increasing flexibility of the elongated chain. The $Au_{28}(SR)_{20}$ is the first cluster of known structure in which trimeric units are observed.

Optical Properties. We calculated both the optical absorption and CD spectra of the $Au_{28}(SMe)_{20}$ cluster. The absorption spectrum shows, in agreement with those reported by Jin and co-workers, an onset of absorption at ca. 700 nm (1.78 eV). The simulated spectrum shows a very similar shape as compared to the experimental[11] one (Figure 3). The calculated CD allows assignment of handedness of the cluster by comparison of the handedness and sign of the signals in the simulated CD spectrum with the experimental spectrum. The CD spectrum is in very good agreement with the experimental one. The transition energies and their sign (in comparison with the experimental values of "enantiomer 2") are in very good agreement (Table 1). We used the right-handed *C*-enantiomer (*C*: clockwise) to compute the CD spectrum. The match in sign of the CD transitions allows assignment of handedness, the compound labeled by Jin and co-workers as "enantiomer 2" is *C*-$Au_{28}(TBBT)_{20}$. The chirality of the cluster is best seen when the trimeric units are removed from the cluster and only the

Table 1. Experimental[11] and Simulated HL and Optical Gaps, Transition Energies and Sign of the Circular Dichroism Spectra of "Enantiomer 2" of $Au_{24}(TBBT)_{20}$ and *C*-$Au_{24}(SMe)_{20}$

	$Au_{28}(TBBT)_{20}$ "Enantiomer 2"	*C*-$Au_{28}(SMe)_2$
HL gap/eV		1.54
optical gap/eV	1.78	1.78
CD transitions (sign)/ nm	340 (−)	330 (−)
	360 (+)	355 (+)
	380 (−)	375 (−)
	400 (+)	415 (+)
	425 (−)	450 (−)
	470 (+)	475 (+)
	ca. 500 (−)	510 (−)
	600 (+), broad and weak	625 (+) and 740 (+)

dx.doi.org/10.1021/jp407494v | J. Phys. Chem. A 2013, 117, 10526−10533

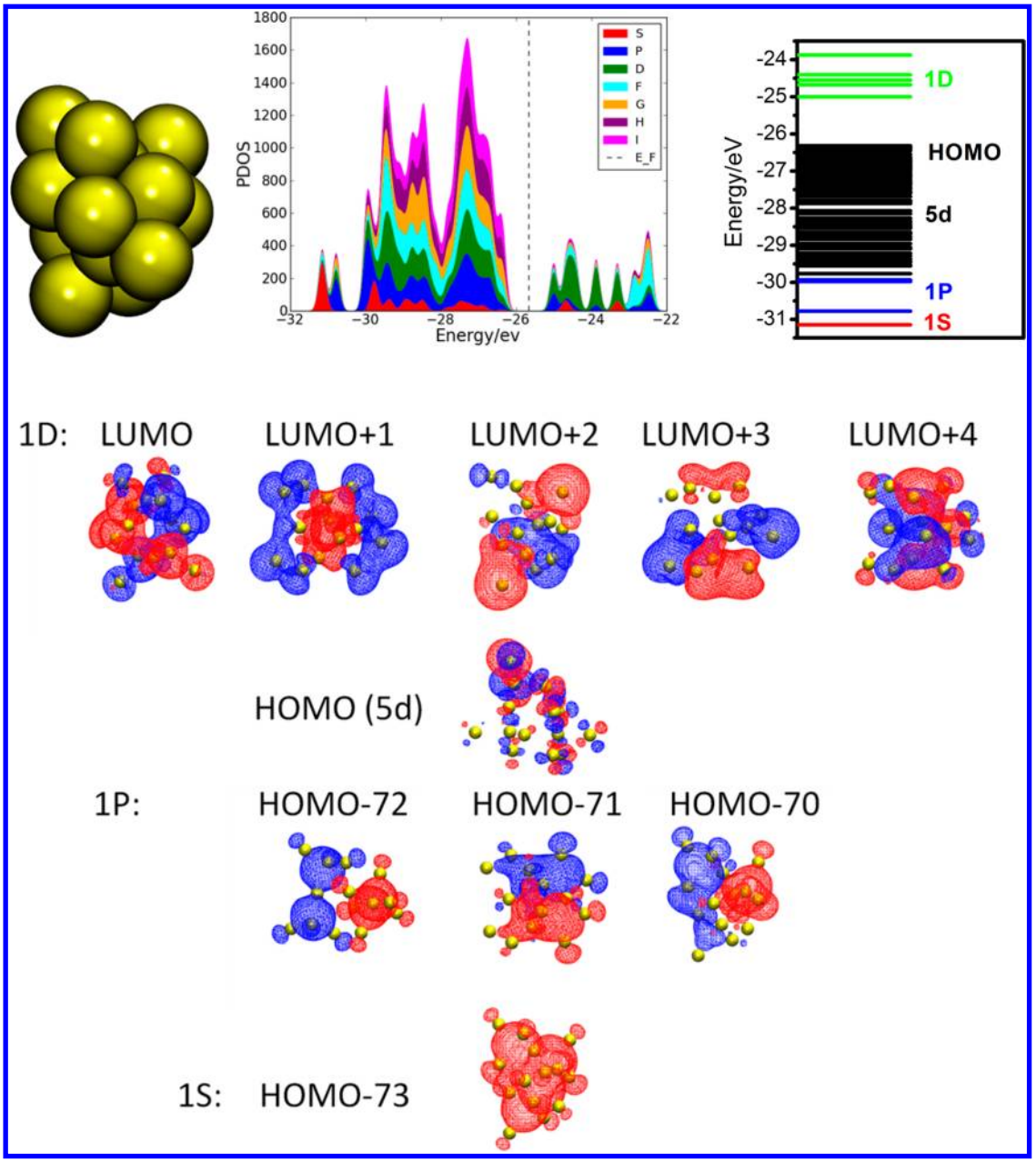

Figure 4. Top: optimized structure and angular momentum resolved PDOS into the COM of the Au_{14}^{6+} cluster and energies of the superatomic 1S-, 1P-, and 1D-states and the 5d band. Colors: red, 1S; blue, 1P; black, 5d; green, 1D. Bottom: visualized KS wave functions of the superatomic orbitals (1S, 1P, 1D) and the HOMO.

dimeric units are considered in view along the principal axis (Figure 3). This procedure is similar to the one used for $Au_{38}(SR)_{24}$ and $Au_{40}(SR)_{24}$.[25,26]

Electronic Structure. Assuming that the cluster is indeed protected by trimeric units, the core is reduced from Au_{20} to Au_{14}. The overall formula of the ligand-protected cluster is $Au_{14}(Au_2(SR)_3)_4(Au_3(SR)_4)_2$. According to the SACM,[16] the cluster has eight valence electrons ($N_e = 14 - 4 - 2 = 8$). This is a "magic number" and a spherical shape of the core is expected. However, the Au_{14} core is not spherical (neither is the Au_{20} core in the $Au_{20}(Au_2(SR)_3)_4(SR)_8$ formula). For analysis of the electronic structure of the Au_{28} cluster, we first turn our focus to the bare core. The Au_{14}^{6+} cluster was optimized, and the electronic states were analyzed by angular momentum resolved projection of the density of states (PDOS) into the center of mass (COM) of the cluster (Figure 4). The first unoccupied states are expected to have D-symmetry (from PDOS), in agreement with 8-electron superatoms (superatomic electronic configuration $1S^2 1P^6 1D^0$).[16,20,41] The occupied states, however, are less defined. Visualization of relevant KS wave functions shows that the HOMO of the cluster is composed of atomic orbitals with d-symmetry, which are localized to the individual atoms and assumed to be 5d-states. Four electronic states are identified as superatomic orbitals: HOMO−73 (1S), and HOMO−72 − HOMO−70 (1P). It is noteworthy that the superatomic orbitals are not the frontier orbitals of the cluster. A similar finding was made by Aikens and co-workers for the tetrahedral Au_4^{2+} cluster (2-electron superatom).[42] The unoccupied orbitals LUMO − LUMO+4 have *D*-symmetry and are

dx.doi.org/10.1021/jp407494v | J. Phys. Chem. A 2013, 117, 10526−10533

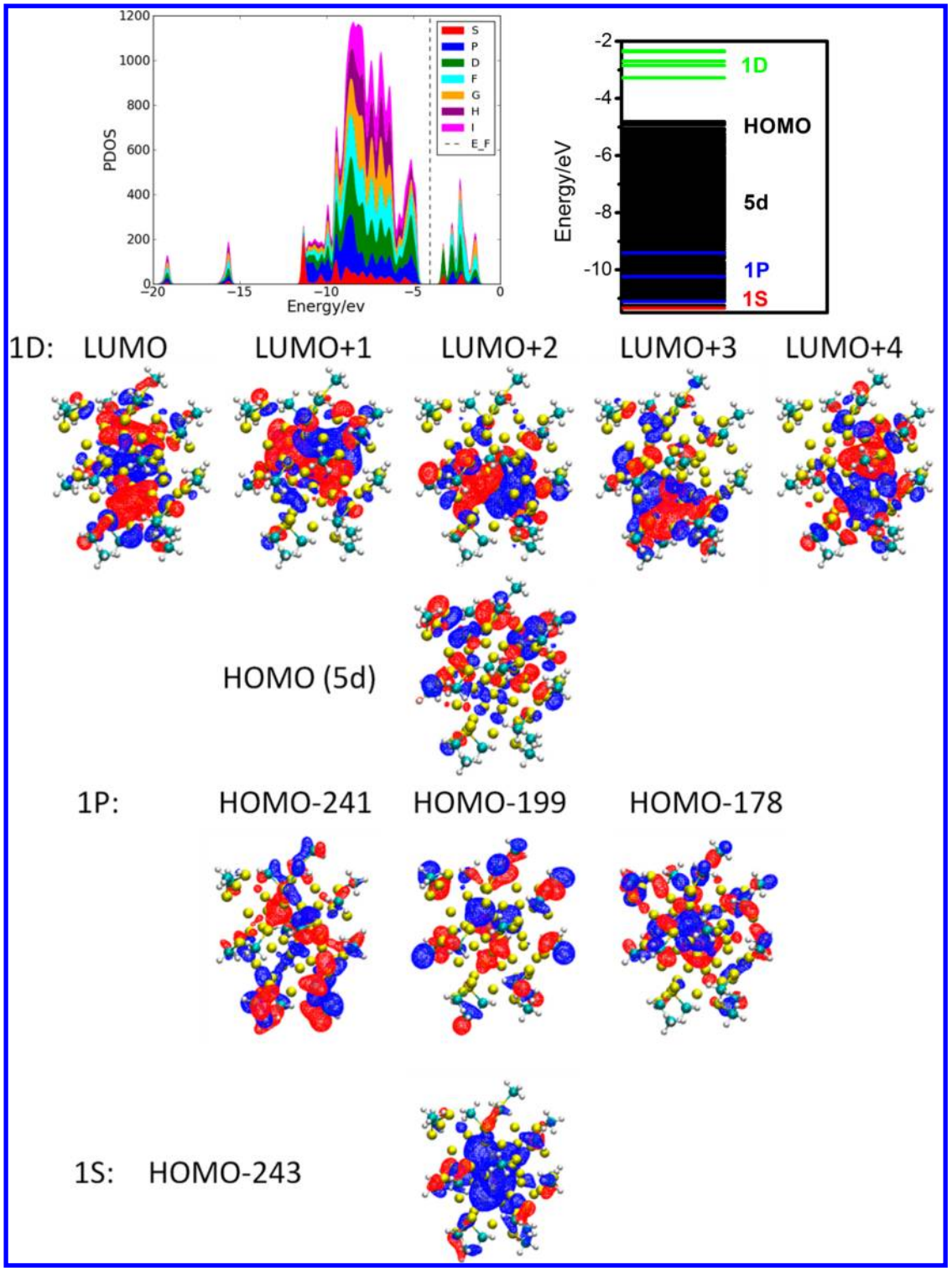

Figure 5. Top: angular momentum resolved PDOS into the center of mass of $Au_{28}(SMe)_{20}$ and energies of the superatomic 1S-, 1P-, and 1D-states and the 5d band (as well as ligands). Colors: red, 1S; blue, 1P; black, 5d (and ligand layer); green, 1D. Bottom: visualized KS wave functions of the superatomic orbitals (1S, 1P, 1D) and the HOMO.

delocalized over the cluster. Overall, the Au_{14}^{6+} cluster can be interpreted as eight-electron superatom. We compared the electronic structure to an "archetypical" eight-electron superatom, Au_{13}^{5+}. This cluster is the core of the $[Au_{25}(SR)_{18}]^-$ cluster[7,41,43] and is both geometrically (icosahedral) and electronically ($1S^21P^6$) stabilized. Comparison reveals that the electronic states in the latter case are more defined than in the Au_{14}^{6+} cluster (Figure S-2, Supporting Information). We relate this to the nonspherical geometry of Au_{14}^{6+}. Both P- and D-states are nondegenerate for the Au_{14}^{6+} cluster, an effect that arises from the distorted shape of the cluster. The comparison also highlights the effects of formal addition of a single, valence electron-free atom (Au^+) to a geometrically and electronically stabilized superatom.

dx.doi.org/10.1021/jp407494v | J. Phys. Chem. A 2013, 117, 10526−10533

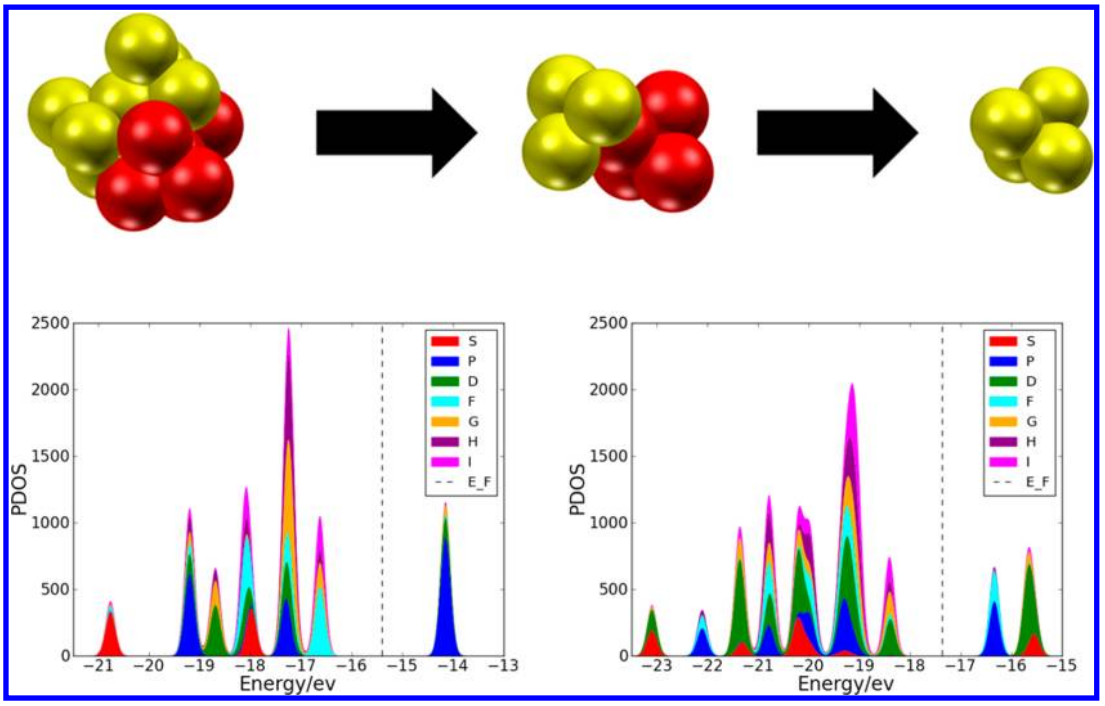

Figure 6. Top: deconstruction of the Au_{14}^{6+} cluster into smaller building blocks, Au_7^{3+} and Au_4^{2+}. The shown structures are optimized, and the constituting building blocks are highlighted with colors. Bottom: angular momentum projected PDOS of Au_4^{2+} (left) and Au_7^{3+} (right).

Electronic structure analysis of the ligand-protected $Au_{28}(SMe)_{20}$ cluster reveals similar results as for Au_{14}^{6+}. The lowest unoccupied states have significant D-symmetry (Figure 5). The HOMO consists of 5d atomic orbitals of the Au atoms in the core. Overall, the electronic situation is less defined due to the presence of the ligand layer. We identified four electronic states with considerable delocalization over the cluster core. The lowest of these (HOMO−243) has S-symmetry. Three nondegenerate states with P-symmetry (HOMO−241, −199, −178) are found as well. The five lowest unoccupied states (LUMO − LUMO+4) have D-symmetry. In all these states (especially the P- and D-states), a considerable distortion from an ideal situation is found. As mentioned above, the cluster is nonspherical and chiral. This low symmetry may have significant effect on the electronic structure. Nevertheless, the $Au_{28}(SMe)_{20}$ cluster can be satisfyingly interpreted as a eight-electron SAC.

It is worthwhile to take the brief detour of having a closer look to the Au_{14} core of the $Au_{28}(SR)_{20}$ cluster. The kernel can be thought of as a dimer of Au_7 subunits. These subunits in turn are trigonal antiprisms and are formed by two tetrahedral units that share one atom (Figure 6, top). In a recent study, the $Au_{40}(SR)_{24}$ cluster was proposed to be formed by a dimer of eight-electron superatoms.[25] Very recently, Cheng et al. proposed a "superatom network" (SAN) concept to explain the structure and stability of the $Au_{20}(SR)_{16}$ cluster.[44] In a similar approach, we discuss the evolution of the Au_{14} core. The eight-electron superatom Au_{14}^{6+} can be thought as a dimer of Au_7^{3+} clusters. These are four-electron clusters. It is known that four-electron clusters can be treated as dimers of 2-electron superatoms within the jellium model.[20] In the present case, the Au_{14}^{6+} cluster would be a tetramer of 2-electron superatoms. This alternative model could explain the stability of the eight-electron cluster even in a nonspherical shape. As discussed above, this assumption does not seem to hold true, because Au_{14}^{6+} can be reasonably well explained as a eight-electron superatom (and the superatomic orbitals span over the two Au_7 subunits). Nevertheless, we studied the building blocks found in the cluster, Au_7^{3+} and the tetrahedral units (which we treated as Au_4^{2+} to fulfill the 2-electron rule).

The Au_4^{2+} cluster is easily identified as a 2-electron superatom. The 1S-state is HOMO−11, and the LUMO, LUMO+1, and LUMO+2 are P-states (Figure S-3, Supporting Information). The HOMO belongs to the 5d band (appears to have F-symmetry in the PDOS due to the tetrahedral symmetry of the cluster; Figure 6, bottom left). These results are in good agreement with those reported earlier.[42] The situation in the Au_7^{3+} cluster, however, is more complicated. Electronic structure analysis reveals an interesting finding: The Au_7^{3+} cluster can be treated as a "supermolecule". The delocalized molecular orbitals of the cluster greatly resemble those found in ethane, with the exception that the Σ_x orbital is higher in energy than the Π'_y and Π'_z orbitals (Figure S-4, Supporting Information). In addition, only the Σ_S and Σ'_S orbitals are occupied. Further studies will show whether or not four-electron clusters of other geometries can be treated as derived from "superethane" molecules.

CONCLUSION

In summary, the $Au_{28}(SMe)_{20}$ as a model system of the recently solved crystal structure of $Au_{28}(TBBT)_{20}$ was studied by means of the density functional theory for the ground-state electronic structure and its time-dependent form to treat the excited states. Bader charge analysis of the optimized structure shows that trimeric units $Au_3(SR)_4$ (besides the known dimers) are present instead of direct binding of thiolates to the kernel of the cluster. This is the first observation of trimeric units in a cluster of known structure. The cluster can be reformulated as $Au_{14}(Au_2(SR)_3)_4(Au_3(SR)_4)_2$. Both the bare core, Au_{14}^{6+}, and the ligand-protected clusters can be interpreted as distorted eight-electron superatom (complex). The distortion arises from the nonspherical shape of the core. TD-DFT was used to

dx.doi.org/10.1021/jp407494v | J. Phys. Chem. A 2013, 117, 10526−10533

compute the ordinary absorption and circular dichroism spectra of the cluster, allowing assignment of handedness by comparison with experimental values.

■ ASSOCIATED CONTENT

Supporting Information

Bader charges of LDA-optimized $Au_{28}(SMe)_{20}$; visualizations of the KS wave functions of Au_{13}^{5+}, Au_4^{2+}, Au_7^{3+}, and ethane; selected structural parameters of the crystal structure of $Au_{28}(TBBT)_{20}$ and the optimized structure of $Au_{28}(SMe)_{20}$. This material is available free of charge via the Internet at http://pubs.acs.org.

■ AUTHOR INFORMATION

Corresponding Author

*S. Knoppe: e-mail, stefan.knoppe@chem.kuleuven.be; tel, +32 16 327 622; fax, +32 16 327 982.

Notes

The authors declare no competing financial interest.

■ ACKNOWLEDGMENTS

S.K. gratefully acknowledges financial support from the German Academic Exchange Service (DAAD). Work in the University of Jyväskylä is supported by the Academy of Finland. The computations were made by using the FGI GRID node "Electra" in the University of Jyväskylä.

■ REFERENCES

(1) Häkkinen, H. The Gold-Sulfur Interface at the Nanoscale. *Nat. Chem.* **2012**, *4*, 443−455.
(2) Aikens, C. M. Electronic Structure of Ligand-Passivated Gold and Silver Nanoclusters. *J. Phys. Chem. Lett.* **2011**, *2*, 99−104.
(3) Maity, P.; Xie, S.; Yamauchi, M.; Tsukuda, T. Stabilized Gold Clusters: From Isolation toward Controlled Synthesis. *Nanoscale* **2012**, *4*, 4027−4037.
(4) Li, G.; Jin, R. Atomically Precise Gold Nanoclusters as New Model Catalysts. *Acc. Chem. Res.* **2013**, *46*, 1749−1758.
(5) Ackerson, C. J.; Powell, R. D.; Hainfeld, J. F. Site-Specific Biomolecule Labeling with Gold Clusters. *Methods Enzymol.* **2010**, *481*, 195−230.
(6) Jadzinsky, P. D.; Calero, G.; Ackerson, C. J.; Bushnell, D. A.; Kornberg, R. D. Structure of a Thiol Monolayer-Protected Gold Nanoparticle at 1.1 A Resolution. *Science* **2007**, *318*, 430−433.
(7) Heaven, M. W.; Dass, A.; White, P. S.; Holt, K. M.; Murray, R. W. Crystal structure of the gold nanoparticle $[N(C_8H_{17})_4][Au_{25}(SCH_2CH_2Ph)_{18}]$. *J. Am. Chem. Soc.* **2008**, *130*, 3754−3755.
(8) Zhu, M.; Eckenhoff, W. T.; Pintauer, T.; Jin, R. Conversion of Anionic $[Au_{25}(SCH_2CH_2Ph)_{18}]^-$ Cluster to Charge Neutral Cluster via Air Oxidation. *J. Phys. Chem. C* **2008**, *112*, 14221−14224.
(9) Qian, H.; Eckenhoff, W. T.; Zhu, Y.; Pintauer, T.; Jin, R. Total Structure Determination of Thiolate-Protected Au_{38} Nanoparticles. *J. Am. Chem. Soc.* **2010**, *132*, 8280−8281.
(10) Zeng, C.; Qian, H.; Li, T.; Li, G.; Rosi, N. L.; Yoon, B.; Barnett, R. N.; Whetten, R. L.; Landman, U.; Jin, R. Total Structure and Electronic Properties of the Gold Nanocrystal $Au_{36}(SR)_{24}$. *Angew. Chem., Int. Ed.* **2012**, *51*, 13114−13118.
(11) Zeng, C.; Li, T.; Das, A.; Rosi, N. L.; Jin, R. Chiral Structure of Thiolate-Protected 28-Gold-Atom Nanocluster Determined by X-ray Crystallography. *J. Am. Chem. Soc.* **2013**, *135*, 10011−10013.
(12) Häkkinen, H.; Walter, M.; Grönbeck, H. Divide and Protect: Capping Gold Nanoclusters with Molecular Gold-Thiolate Rings. *J. Phys. Chem. B* **2006**, *110*, 9927−9931.
(13) Jiang, D.-e.; Chen, W.; Whetten, R. L.; Chen, Z. What Protects the Core When the Thiolated Au Cluster is Extremely Small? *J.Phys. Chem. C* **2009**, *113*, 16983−16987.
(14) Tlahuice, A.; Garzon, I. L. On the Structure of the $Au_{18}(SR)_{14}$ Cluster. *Phys. Chem. Chem. Phys.* **2012**, *14*, 3737−3740.
(15) Tlahuice, A.; Garzon, I. L. Structural, Electronic, Optical, and Chiroptical Properties of Small Thiolated Gold Clusters: The Case of Au_6 and Au_8 Cores Protected with Dimer $[Au_2(SR)_3]$ and Trimer $[Au_3(SR)_4]$ Motifs. *Phys. Chem. Chem. Phys.* **2012**, *14*, 7321−7329.
(16) Walter, M.; Akola, J.; Lopez-Acevedo, O.; Jadzinsky, P. D.; Calero, G.; Ackerson, C. J.; Whetten, R. L.; Grönbeck, H.; Häkkinen, H. A Unified View of Ligand-Protected Gold Clusters as Superatom Complexes. *Proc. Natl. Acad. Sci.* **2008**, *105*, 9157−9162.
(17) Knight, W.; Clemenger, K.; de Heer, W.; Saunders, W.; Chou, M.; Cohen, M. Electronic Shell Structure and Abundances of Sodium Clusters. *Phys. Rev. Lett.* **1984**, *52*, 2141−2143.
(18) Cohen, M. L.; Chou, M. Y.; Knight, W. D.; de Heer, W. A. Physics of Metal Clusters. *J. Phys. Chem.* **1987**, *91*, 3141−3149.
(19) Martin, T. P.; Bergmann, T.; Goehlich, H.; Lange, T. Shell Structure of Clusters. *J. Phys. Chem.* **1991**, *95*, 6421−6429.
(20) Koskinen, M.; Lipas, P. O.; Manninen, M. Electron-Gas Clusters: The Ultimate Jellium Model. *Z. Phys. D* **1995**, *35*, 285−297.
(21) Pei, Y.; Gao, Y.; Zeng, X. C. Structural Prediction of Thiolate-Protected Au_{38}: A Face-Fused Bi-Icosahedral Au Core. *J. Am. Chem. Soc.* **2008**, *130*, 7830−7832.
(22) Lopez-Acevedo, O.; Tsunoyama, H.; Tsukuda, T.; Häkkinen, H.; Aikens, C. M. Chirality and Electronic Structure of the Thiolate-Protected Au_{38} Nanocluster. *J. Am. Chem. Soc.* **2010**, *132*, 8210−8218.
(23) Cheng, L.; Ren, C.; Zhang, X.; Yang, J. New Insight into the Electronic Shell of $Au_{38}(SR)_{24}$: A Superatomic Molecule. *Nanoscale* **2013**, *5*, 1475−1478.
(24) Häkkinen, H.; Manninen, M. Electronic-Structure-Induced Deformations of Liquid Metal Clusters. *Phys. Rev. B* **1995**, *52*, 1540−1543.
(25) Malola, S.; Lehtovaara, L.; Knoppe, S.; Hu, K. J.; Palmer, R. E.; Bürgi, T.; Häkkinen, H. $Au_{40}(SR)_{24}$ Cluster as a Chiral Dimer of 8-Electron Superatoms: Structure and Optical Properties. *J. Am. Chem. Soc.* **2012**, *134*, 19560−19563.
(26) Dolamic, I.; Knoppe, S.; Dass, A.; Bürgi, T. First Enantioseparation and Circular Dichroism Spectra of Au_{38} Clusters Protected by Achiral Ligands. *Nat. Commun.* **2012**, *3*, 798.
(27) Knoppe, S.; Dolamic, I.; Dass, A.; Bürgi, T. Separation of Enantiomers and CD Spectra of $Au_{40}(SCH_2CH_2Ph)_{24}$: Spectroscopic Evidence for Intrinsic Chirality. *Angew. Chem., Int. Ed.* **2012**, *51*, 7589−7591.
(28) Schaaff, T. G.; Knight, G.; Shafigullin, M. N.; Borkman, R. F.; Whetten, R. L. Isolation and Selected Properties of a 10.4 kDa Gold: Glutathione Cluster Compound. *J. Phys. Chem. B* **1998**, *102*, 10643−10646.
(29) Schaaff, T. G.; Whetten, R. L. Giant gold-glutathione cluster compounds: Intense optical activity in metal-based transitions. *J. Phys. Chem. B* **2000**, *104*, 2630−2641.
(30) Yao, H.; Miki, K.; Nishida, N.; Sasaki, A.; Kimura, K. Large Optical Activity of Gold Nanocluster Enantiomers Induced by a Pair of Optically Active Penicillamines. *J. Am. Chem. Soc.* **2005**, *127*, 15536−15543.
(31) Gautier, C.; Taras, R.; Gladiali, S.; Bürgi, T. Chiral 1,1′-Binaphthyl-2,2′-dithiol-Stabilized Gold Clusters: Size Separation and Optical Activity in the UV-Vis. *Chirality* **2008**, *20*, 486−493.
(32) Gautier, C.; Bürgi, T. Chiral Gold Nanoparticles. *ChemPhysChem* **2009**, *10*, 483−492.
(33) Knoppe, S.; Kothalawala, N.; Jupally, V. R.; Dass, A.; Bürgi, T. Ligand Dependence of the Synthetic Approach and Chiroptical Properties of a Magic Cluster Protected with a Bicyclic Chiral Thiolate. *Chem. Commun.* **2012**, *48*, 4630−4632.
(34) Zhu, M.; Qian, H.; Meng, X.; Jin, S.; Wu, Z.; Jin, R. Chiral Au Nanospheres and Nanorods: Synthesis and Insight into the Origin of Chirality. *Nano Lett.* **2011**, *11*, 3963−3969.
(35) Mortensen, J.; Hansen, L.; Jacobsen, K. Real-Space Grid Implementation of the Projector Augmented Wave Method. *Phys. Rev. B* **2005**, *71*.

(36) Enkovaara, J.; Rostgaard, C.; Mortensen, J. J.; Chen, J.; Dulak, M.; Ferrighi, L.; Gavnholt, J.; Glinsvad, C.; Haikola, V.; Hansen, H. A.; et al. Electronic Structure Calculations with GPAW: A Real-Space Implementation of the Projector Augmented-Wave Method. *J. Phys. Condens. Mater.* **2010**, *22*, 253202.
(37) Perdew, J. P.; Burke, K.; Ernzerhof, M. Generalized Gradient Approximation Made Simple. *Phys. Rev. Lett.* **1996**, *77*, 3865−3868.
(38) Perdew, J. P.; Burke, K.; Ernzerhof, M. Generalized Gradient Approximation Made Simple [Phys. Rev. Lett. 77, 3865 (1996)]. *Phys. Rev. Lett.* **1997**, *78*, 1396−1396.
(39) Bader charge analysis: The Henkelman Group, http://theory.cm.utexas.edu/henkelman/research/bader/ (accessed Sep 4, 2013).
(40) Tang, W.; Sanville, E.; Henkelman, G. A Grid-Based Bader Analysis Algorithm without Lattice Bias. *J. Phys. Condens. Mater.* **2009**, *21*, 084204.
(41) Akola, J.; Walter, M.; Whetten, R. L.; Häkkinen, H.; Grönbeck, H. On the Structure of Thiolate-Protected Au_{25}. *J. Am. Chem. Soc.* **2008**, *130*, 3756−3757.
(42) Ivanov, S. A.; Arachchige, I.; Aikens, C. M. Density Functional Analysis of Geometries and Electronic Structures of Gold-Phosphine Clusters. The Case of $Au_4(PR_3)_4^{2+}$ and $Au_4(\mu_2\text{-}I)_2(PR_3)_4$. *J. Phys. Chem. A* **2011**, *115*, 8017−8031.
(43) Zhu, M.; Aikens, C. M.; Hollander, F. J.; Schatz, G. C.; Jin, R. Correlating the Crystal Structure of a Thiol-Protected Au_{25} Cluster and Optical Properties. *J. Am. Chem. Soc.* **2008**, *130*, 5883−5885.
(44) Cheng, L.; Yuan, Y.; Zhang, X.; Yang, J. Superatom Networks in Thiolate-Protected Gold Nanoparticles. *Angew. Chem., Int. Ed.* **2013**, *52*, 9035−9039.